Journal of Computer-Aided Molecular Design, 11 (1997) 9–20
ESCOM

J-CAMD 377

Molecular modeling of the neurophysin I/oxytocin complex

R. Kaźmierkiewicz, C. Czaplewski, B. Lammek and J. Ciarkowski*

Faculty of Chemistry, University of Gdańsk, Sobieskiego 18, PL-80-952 Gdańsk, Poland

Received 12 June 1996
Accepted 27 August 1996

Keywords: Protein–ligand interactions; Molecular dynamics; AMBER 4.1; Allosteric communication

Summary

Neurophysins I and II (NPI and NPII) act in the neurosecretory granules as carrier proteins for the neurophyseal hormones oxytocin (OT) and vasopressin (VP), respectively. The NPI/OT functional unit, believed to be an $(NPI/OT)_2$ heterotetramer, was modeled using low-resolution structure information, viz. the C^{α} carbon atom coordinates of the homologous NPII/dipeptide complex (file 1BN2 in the Brookhaven Protein Databank) as a template. Its all-atom representation was obtained using standard modeling tools available within the INSIGHT/Biopolymer modules supplied by Biosym Technologies Inc. A conformation of the NPI-bound OT, similar to that recently proposed in a transfer NOE experiment, was docked into the ligand-binding site by a superposition of its Cys^1-Tyr^2 fragment onto the equivalent portion of the dipeptide in the template. The starting complex for the initial refinements was prepared by two alternative strategies, termed Model I and Model II, each ending with a ~100 ps molecular dynamics (MD) simulation in water using the AMBER 4.1 force field. The free homodimer NPI_2 was obtained by removal of the two OT subunits from their sites, followed by a similar structure refinement. The use of Model I, consisting of a constrained simulated annealing, resulted in a structure remarkably similar to both the NPII/dipeptide complex and a recently published solid-state structure of the NPII/OT complex. Thus, Model I is recommended as the method of choice for the preparation of the starting all-atom data for MD. The MD simulations indicate that, both in the homodimer and in the heterotetramer, the 3_{10}-helices demonstrate an increased mobility relative to the remaining body of the protein. Also, the C-terminal domains in the NPI_2 homodimer are more mobile than the N-terminal ones. Finally, a distinct intermonomer interaction is identified, concentrated around its most prominent, although not unique, contribution provided by an H-bond from Ser^{25} O^{γ} in one NPI unit to Glu^{81} O^{ε} in the other unit. This interaction is present in the heterotetramer $(NPI/OT)_2$ and absent or weak in the NPI_2 homodimer. We speculate that this interaction, along with the increased mobility of the 3_{10}-helices and the carboxy domains, may contribute to the allosteric communication between ligand binding and NPI dimerization.

Introduction

The nonapeptide hormones oxytocin, CYIQNCPLG-NH_2 (OT), and vasopressin, CYFQNCPRG-NH_2 (VP), while transported in the posterior pituitary, are packaged in relatively high concentrations (>0.1 M) [1] in the neurosecretory granules (NSG) as associates 1:1 (per molecular basis) with disulfide-rich proteins known as neurophysin I (NPI) and neurophysin II (NPII), respectively. The specific OT/NPI and VP/NPII complexes result from the respective common precursors [2,3], even though the two NPs bind in vitro with either hormone as well as with a number of small N-terminal peptide analogues [4–6]. The interactions between the NPs and the hormone segments within the precursors seem to be similar to those in the complexes and essential for a correct folding of the precursors and pairing of the disulfides [7–11]. The major function of the NPs is to serve as carrier proteins for the hormones until the latter are dissociated upon secretion into the blood. Both the NPs are small disulfide-rich proteins of 93–95 amino acid residues per monomer, consisting of two highly homological domains, supported by seven disulfide bridges: three bridges per domain plus an interdomain one.

Two solid-state structures of NPs are currently available: the first one for the NPII/dipeptide complex [12]

*To whom correspondence should be addressed.

A

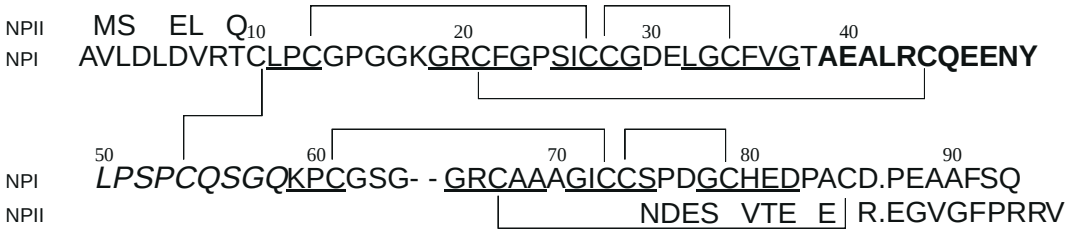

B

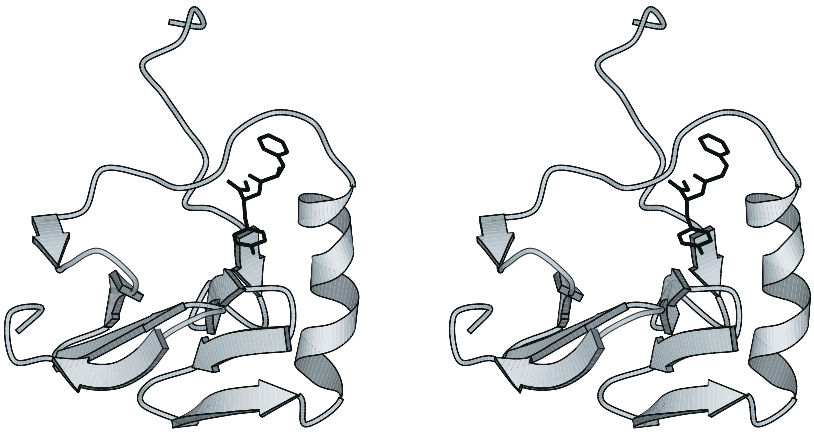

Fig. 1. (A) The sequences of bovine NPI and NPII. The β-strands are underlined, the 3_{10} helix is in bold and the interdomain connection is in italic. The C-terminal fragment, not included in the solid-state structure [12], is separated with a dot. The homological fragments in the amino and carboxyl domains are aligned vertically one under the other. (B) The structure of the NPII/dipeptide heterodimer [12] built up from the C^{α} carbon coordinates (file 1BN2 in the Brookhaven PDB). The NPII molecule is made up of two highly homological domains, composed of similar four-stranded antiparallel β-sheets. In the amino domain the β-sheet is immediately followed by a three-turn 3_{10} helix, having no match in the carboxyl domain. Both domains are connected by a relatively loose backbone fragment, supported by an *inter*domain disulfide bridge C10–C54. The remaining six disulfide bridges crosslink the *intra*domain residues: bridges 13–27, 21–44 and 28–34 within the amino domain and bridges 61–73, 67–85 and 74–79 within the carboxyl domain. The dipeptide ligand, represented by a stick model, is seen in the binding loop (ENYLPSPC, 47–54) composed of the end of the 3_{10} helix (AEALRCQEENY, 39–49) and the beginning of the interdomain connection (LPSPCQSGQ, 50–58).

and the other one just released for the NPII/OT (cross) complex [13]. Both the three-dimensional structures, while confirming extensive structural homologies and virtually identical binding modes for OT and the dipeptide analogue, also provide details on conformations of the ligands, locations of the binding sites, and details regarding the modes of interactions between the NPs and the ligands, see Fig. 1.

Our current interest is in the de novo modeling of protein–ligand interactions, starting from a sequence homology and/or low-resolution structural information. To this aim, we have recently simulated the NPII/dipeptide complex [14], using merely the C^{α} trace as a starting frame, which was at the same time the only data deposited by Chen et al. [12] in the Brookhaven Protein Databank (PDB) [15] as file 1BN2. Our simulation led to a complex that overlapped well with the reference C^{α} trace and also perfectly reproduced all the key interactions between the protein and the ligand. In this work we extend the modeling and the MD simulation from the NPII/dipeptide complex [12] onto the $(NPI/OT)_2$ heterotetramer. We also employ and evaluate a new modeling technique based on constrained simulated annealing (CSA).

TABLE 1
PROTOCOL FOR CSA IN VACUO

Stage	Steps (fs)	Duration (ps)	T_0 [a] (K)	TAUTP[b]
1 Fast heating	0–1000	1	0–1200 (linear)	0.2
2 Hot equilibration	1001–3000	2	1200	0.2
3 Slow cooling (a)	3001–11 000	8	0	4
4 Slow cooling (b)	11 001–13 000	2	0	1
5 Slow cooling (c)	13 001–18 500	5.5	0	0.5
6 Slow cooling (d)	18 501–20 000	1.5	0	0.05

[a] T_0 is the temperature of a fictitious environment, serving, together with parameter TAUTP (see footnote b) as a control during the simulated heating (cooling) of the object.
[b] TAUTP is a temperature relaxation time [21] inversely related to the heat conductivity between the object and the generic environment.

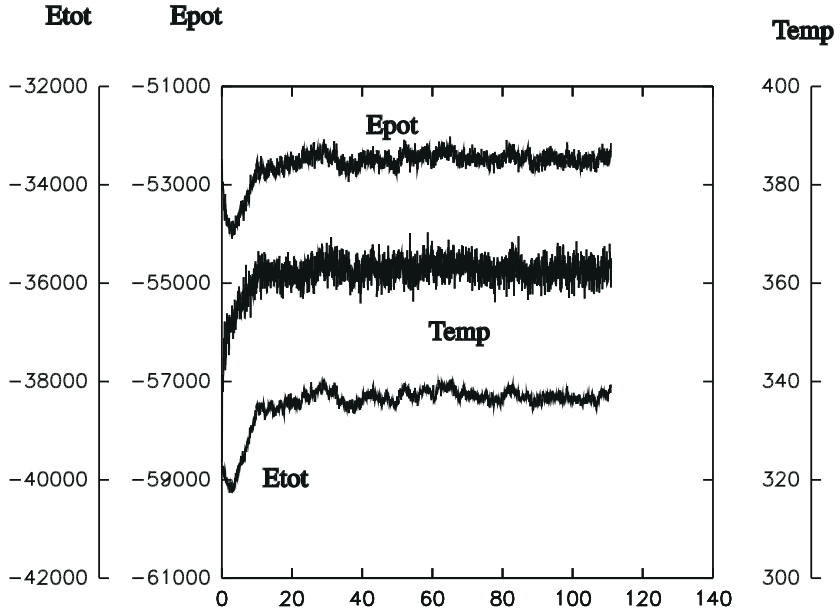

Fig. 2. Evolution of the total energy, the potential energy and the temperature over 111 ps for Model I.

Methods

The starting all-atom (NPII/dipeptide)$_2$ heterotetramer was used as a template. It was generated from the respective C^{α} trace (file 1BN2, Brookhaven PDB [15]) as described in detail in our former work [14]. The units 1 and 2 from the 1BN2 C^{α} coordinate list were utilized in this work. The NPII molecules were mutated into NPI ones using the Biopolymer module from the SYBYL [16] suite of programs. Subsequently, OT in the reportedly NPI-bound conformation [17] was superimposed twice, using its Cys^1-Tyr^2 fragment, onto the equivalent portions of the dipeptide ligands in the template, followed by removing both the dipeptide ligand molecules from the structure. The Tyr^2 side-chain conformations in both OT molecules were corrected from $\chi_1 \cong 90°$ [17] to $\chi_1 \cong -60°$, in accordance with convincing arguments in a recent paper of Breslow et al. [18]. Consecutively, the (NPI/OT)$_2$ heterotetramer was processed in the following two ways, referred to as Model I and Model II.

Model I

The starting (NPI/OT)$_2$ heterotetramer was subjected to 20 000 steps of minimization in vacuo with all the C^{α} atomic positions frozen and coincident with the respective mutant coordinates (see above) in the NPII/dipeptide

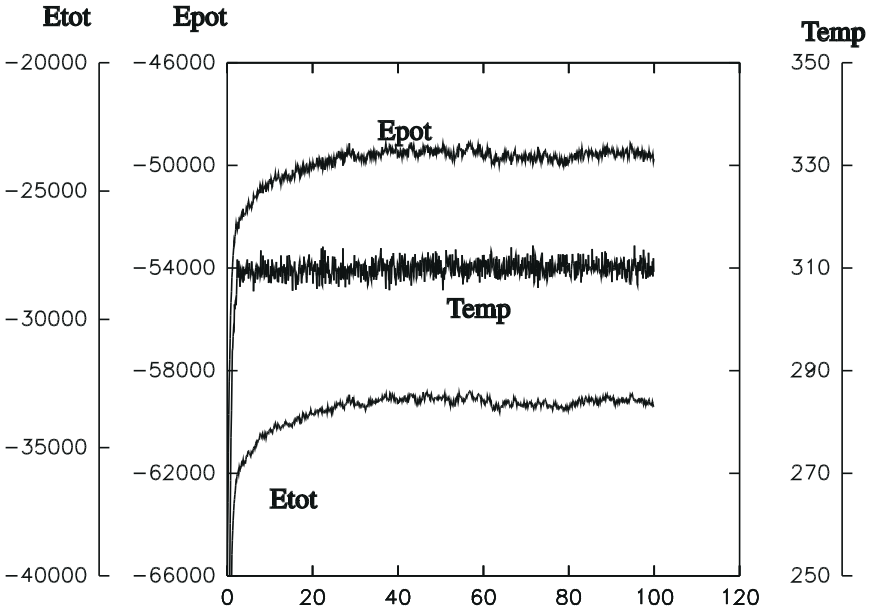

Fig. 3. Evolution of the total energy, the potential energy and the temperature over 100 ps for Model II.

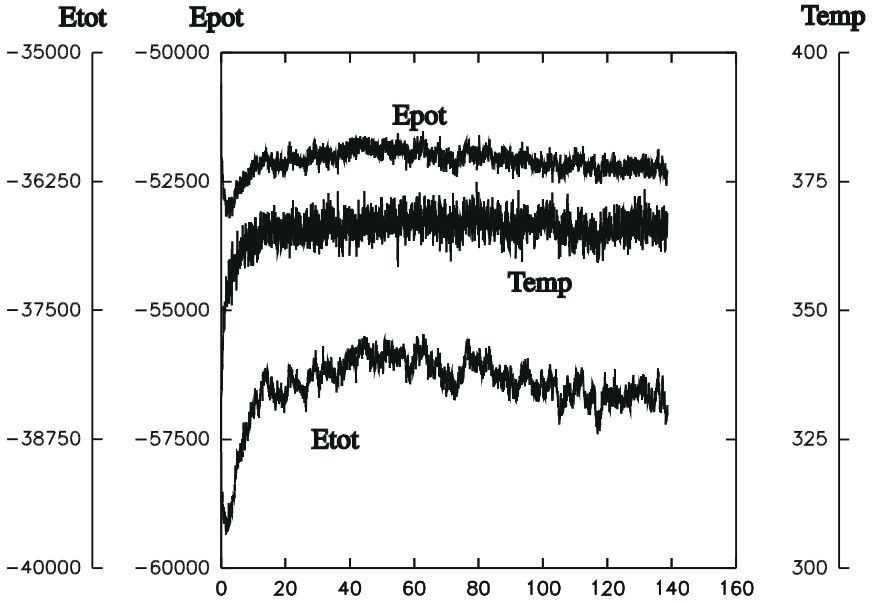

Fig. 4. Evolution of the total energy, the potential energy and the temperature over 139 ps for the homodimer.

complex (file 1BN2 [15]). This and other subsequent minimizations were carried out in the steepest descent mode through the first 1000 steps, followed by the conjugate gradient mode for the remaining steps. This and all subsequent operations in vacuo (see below) were executed using linearly distance-dependent dielectric permittivity. Conversely, all simulations in explicit water always used constant dielectric (=1) and periodic boundary conditions. A default residue-based cutoff value of 8 Å was used. In Model I the structure was prepared for MD using the CSA procedure (SANDER) as implemented in the AMBER 4.1 suite of programs [19]. During execution of CSA, all the C^{α} atoms were also kept frozen in their starting positions (see above) and, in addition, suitable force constants were imposed on the improper dihedrals and the peptide bonds, in order to maintain all chiral centers and peptide geometries, respectively, undisturbed. With all the constraints in effect, the CSA was executed in vacuo. The details of the CSA protocol are given in Table 1.

Having finished the CSA, the minimization in vacuo (20 000 steps) was carried out again. This was followed by 20 000 cycles of minimization in a water box with the C^{α} atoms still locked in their starting positions. A typical box contained approximately 5500–5600 TIP3P water molecules [20] which, together with the protein, made up some 18 000–18 500 atoms. For a typical box size of 88 Å $\times$ 50 Å $\times$ 47 Å this would correspond to a concentration of ca. 8.0×10^{-3} mol dm^{-3}. Subsequently, the C^{α} atoms were set free and another 20 000 cycles of minimization in water were executed. After the energy was minimized, the system was thermally equilibrated. This consisted of a number of MDs with the total energy constant and the velocities assigned from the Maxwellian distribution, at temperatures of 10, 100, 200 and 300 K (10 runs 0.1 ps long for each temperature). The resampling of velocities from the Maxwell–Boltzmann distribution was applied during the equilibration to remove hot and/or cold spots (high/low levels of kinetic energy localized in small areas). Having completed thermal equilibration, the system was subjected to 111 ps of MD at a temperature of 300 K, with the SHAKE option on, which enabled a time step of 1 fs.

Homodimer

The initial NPI_2 homodimer was obtained by removing both OT molecules from their binding sites. It was sub-

→

Fig. 5. The contour plot illustrates the evolution of the geometry in Model I, represented by the C^{α} sequential positions along the vertical axis, over the time range of 111 ps (horizontal axis). The contours are drawn every 2 Å. The deviations are measured with respect to the C^{α} carbon positions in the NPII mutant (file 1BN2 in the Brookhaven PDB) that also served as the template for the starting structure (see the Methods section). The projection of the contour map onto the vertical axis signifies the distribution of the time-averaged mobility along the sequence represented by the C^{α} carbon atoms. The projection of the contour map onto the horizontal axis scores the build-up of the rms deviation over the 100 ps of MD. The N-terminal residues 1–6 were disordered in any monomer in the template. As expected, they fluctuate most significantly in MD. Some exposed loops are also quite mobile. Substantial fluctuations are seen in the OT C-terminal tails (residues 7–9) and somewhat smaller ones in the exposed parts of the tocin ring (residues 3–5). All these features are apparent both in the contour map and along the vertical axis. In order to disregard the effect of those clearly excessive fluctuations from disordered parts, the rms build-up (horizontal axis) is also drawn for the system with the NPI residues 1–6 and all OT residues disregarded.

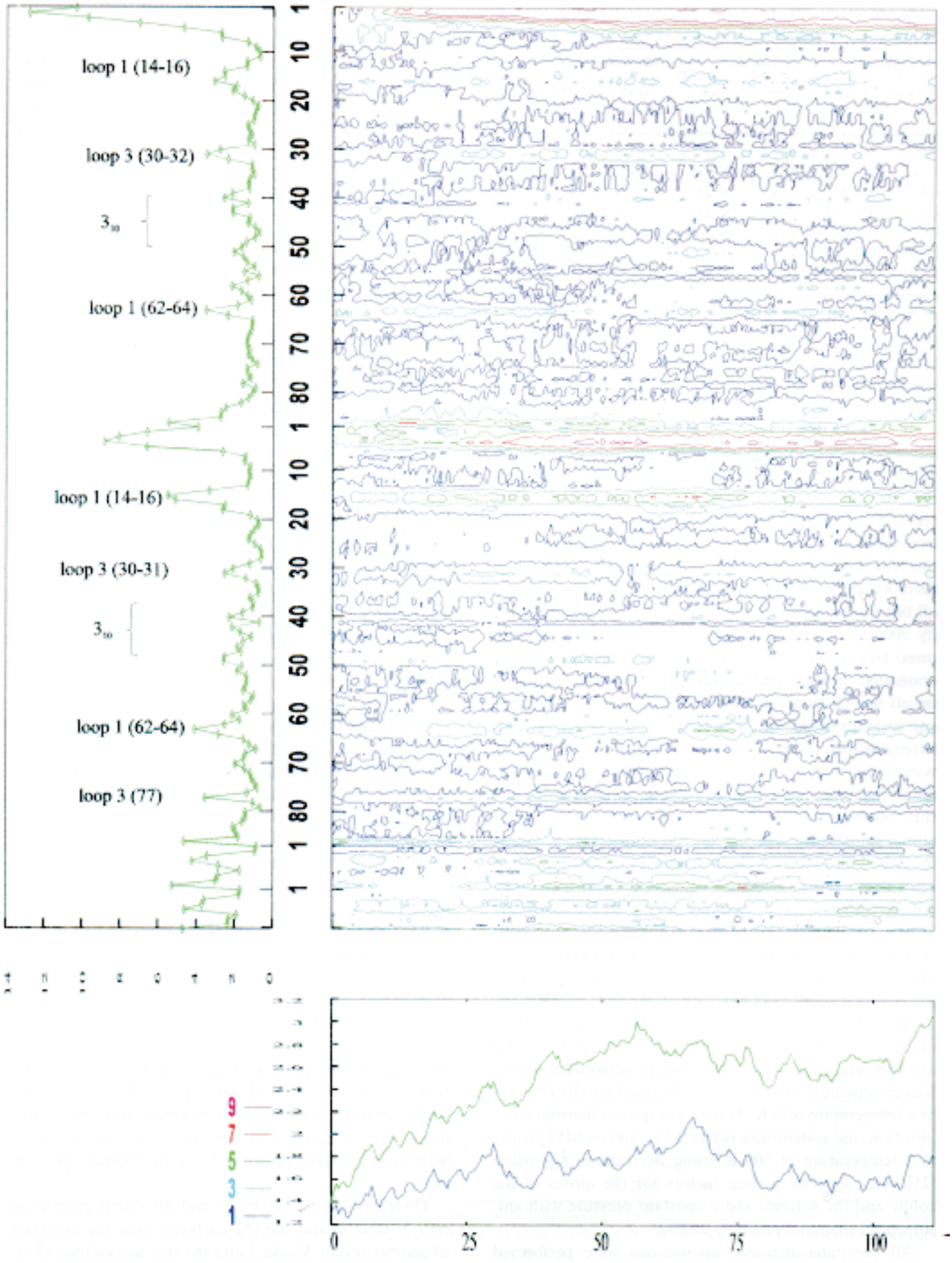
loop 1 (14-16)
loop 3 (30-32)
loop 1 (62-64)
loop 1 (14-16)
loop 3 (30-31)
loop 1 (62-64)
loop 3 (77)
0
25
50
75
100

TABLE 2
SELECTED HYDROGEN BOND PATTERNS IN THE COMPLEX

Neurophysin		Oxytocin		Monomer 1		Monomer 2		Neurophysin monomer 1	Neurophysin monomer 2	Bond distance	% of time occupied
Residue	Atom	Residue	Atom	Bond distance	% of time occupied	Bond distance	% of time occupied				
Ser^{52}	O (A)	Cys^{1}	N (D)	2.8 (1)[3]	100	2.8 (1)	100	Ser^{25} OG (D)	Glu^{81} OE1 (A)	2.7 (2)	100
Leu^{50}	O (A)	Cys^{1}	N (D)	2.8 (1)	100	2.8 (1)	100	Ser^{25} OG (D)	Glu^{81} OE2 (A)	3.5 (4)	48
Glu^{47}	O (A)	Cys^{1}	N (D)	2.8 (1)	69	2.8 (1)	62	Glu^{81} OE1 (A)	Ser^{25} OG (D)	3.0 (4)	82
Glu^{47}	OE1 (A)	Cys^{1}	N (D)	2.7 (1)	100	2.8 (1)	100	Glu^{81} OE2 (A)	Ser^{25} OG (D)	3.1 (5)	62
Cys^{54}	N (D)	Cys^{1}	O (A)	3.0 (2)	48	2.9 (2)	96				
Cys^{44}	O (A)	Tyr^{2}	OH (D)	2.8 (2)	100	2.9 (2)	100				
Cys^{54}	O (A)	Ile^{3}	N (D)	–	0	3.5 (3)	72				

A: acceptor; D: donor; standard deviations are given in parentheses.

sequently processed in accordance with Model I. The MD simulation took 139 ps.

Model II

This model employed slightly modified procedures described in our former work (Ref. 14). The initial $(NPI/OT)_2$ heterotetramer was first subjected to two short constrained minimizations in vacuo: 1000 cycles with only the NPI atoms (all but the C^{α} ones) allowed to move and then 300 cycles with both the NPI and OT atoms (again all but the C^{α} ones) allowed to move. This was followed by 300 cycles with all the OT atoms (including the C^{α} ones) free to move. Subsequently, the minimization was continued through 1000 cycles with constraints imposed on all the C^{α} atoms in NP and the C^{α} atoms in the first two residues of OT. In the subsequent step the $(NPI/OT)_2$ heterotetramer was immersed in a rectangular box of water with the minimum thickness of the solvent shell along the X, Y and Z axes equal to 8 Å. The energy was then minimized through 1000 cycles with all the solute atoms constrained. Having still the constraints in effect, this was followed by a short 1 ps MD at constant total energy and initial velocities calculated from the forces. Another 100 cycles of minimization with all the solute atoms constrained were executed. Finally, the minimization was continued through 10 000 cycles with constraints imposed on all the C^{α} atoms in NP and the C^{α} atoms in the first two residues of OT.

After the energy was minimized, the system was thermally equilibrated. This consisted of ten 0.5 ps long MD at a temperature of 10 K with constant volume and velocities assigned each time from the Maxwellian distribution at a temperature of 5 K. Having completed thermal equilibration, the system was subjected to 100 ps MD proper at a temperature of 300 K using Berendsen's algorithm [21], with separate scaling factors for the atoms in the solute and the solvent, and a constant pressure with anisotropical diagonal position scaling.

All computer-intensive calculations were performed either on a CRAY Y-MP/EL-98 at the Interdisciplinary Center for Mathematical and Computer Modelling at the University of Warsaw (ICM UW) or on an SGI Power Challenge $4 \times$ R8000 at the Informatics Center of the Metropolitan Academic Network (IC MAN) in Gdańsk. A typical 100 ps dynamics needed 250 h of CPU time on the CRAY and 100 h of CPU time on the SGI Power Challenge. Interactive modeling, both in Warsaw and in Gdańsk, was done using SGI INDY or INDYGO workstations. The images for presentation were prepared using the program MolScript [22] (Figs. 1B, 8, 9 and 10) or RasMol [23] (Figs. 11 and 12).

Results

The time evolution of energy for Model I and Model II is shown in Figs. 2 and 3, respectively. It is seen that in Model I the starting $(NPI/OT)_2$ heterotetramer needs about 15 ps for achieving reasonably stabilized fluctuations in time. This is also true for the homodimer $(NPI)_2$ as illustrated in Fig. 4. On the other hand, the starting $(NPI/OT)_2$ heterotetramer compatible with Model II needs (as seen in Fig. 3) more than 30 ps for achieving reasonably stabilized fluctuations in time. The evolution of the geometries for Model I, Model II and for the $(NPI)_2$ homodimer is shown in Figs. 5, 6 and 7, respectively. The intense changes in energy at the start of each MD simulation do not correlate with the changes in geometry. Thus, the initial energy changes may likely be due to an accommodation and/or penetration of water molecules by the protein surface and/or into the protein body. In the case of Model II the contributions to these energy changes may have also resulted from the accommodation of the side chains whose initial packing, as we believe, could have been far from an optimal one, vide infra.

Disregarding the externally and disorderly protruding NPI N-termini and the OT carboxyl tails, the evolution of geometries for Model I and the free homodimer (Figs.

5 and 7, respectively) illustrates that, on the 100 ps time scale, the motions are mainly local and at least some of them consist of fluctuations tending over a period of ca. 100 ps to recover back to the initial ranges of deviations (see e.g. loop 3 in the amino domain of the first monomer of $(NPI/OT)_2$, loop 1 in the amino domain of the second monomer of $(NPI/OT)_2$, or the rms build-up, all features in Fig. 5; see also loop 3 in the amino domain of the first monomer of NP_2, Fig. 7). Simultaneously, it is seen that, apart from those excluded above, the most flexible parts of the complex are the ligand-binding sites, further extending on the whole 3_{10} helix and the interdomain connection and, in the case of the homodimer, also on the carboxyl domains. In contrast, the evolution of the geometry in Model II (see Fig. 6) indicates that the C-terminal NPI domains drift away from their starting geometries (prior to MD), and this feature, when compared with the completely different behavior of Model I, may be indicative of the initial side-chain packing resulting from this model being far from an optimal one and, at the same time, indicative of a greater sensitivity of the carboxyl domain than the amino domain to modeling conditions viewed both in terms of the technique used and the true structural environment.

A detailed inspection of the final structure and the associated interactions arising from Model I (see Fig. 8 and Table 2) identifies two sets of symmetry-related intermonomer interactions, concentrated around the most prominent, although not unique, contributions made by H-bonds from Ser^{25} O^{γ} in one NPI unit to Glu^{81} O^{ε} in the other unit (and vice versa), and by nonpolar interactions between the side chains of Val^{36} in one NPI unit and Ile^{72} in the other unit (and vice versa) (see Fig. 8). These interactions are accompanied by many other (mainly van der Waals) contributions involving the amino domain second loop/third strand link (GPSI, 23–26) and the fourth strand/3_{10} helix base (VGT, 36–38) in the first (second) NPI unit, and the carboxyl domain third (AGICCS, 70–75) and fourth strands (HEDP, 80–83) in the second (first) NPI unit. The contact distances among the relevant side chains range between 3 and 8 Å. By a comparison of Figs. 8 and 10, it may be seen that these sets of interactions are more prominent in the $(NPI/OT)_2$ heterotetramer than in the NPI_2 homodimer. Altogether, this may point to a possible ligand-induced interdomain interunit communication and to a role it may play in an interdependence between the ligand binding and the NPI dimerization, vide infra.

The N-terminal NPI domains consistently appear less mobile than their C-terminal counterparts. This feature is reflected not only in Figs. 5, 6 and 7 but also in the fact that the structures resulting from the time-averaging of the last 20 ps of the simulations (Figs. 8, 9 and 10 for Model I, Model II and the homodimer, respectively) overlap markedly more poorly onto each other and onto the $(NPII/dipeptide)_2$ C^{α} trace template (structure 1BN2) with their C-terminal than with their N-terminal domains, as is illustrated in Figs. 8, 9 and 10 and Table 3. The only exception is the $(NPI/OT)_2$/template pair in which the amino and carboxyl domain pairs overlap well and to the same extent.

Table 3, together with Figs. 5 and 6, also shows that Model II leads to results of far inferior quality than Model I. In particular, it is seen that the β-sheets making the carboxyl domains have drifted away considerably from the starting C^{α} trace template (see Fig. 6).

Figure 11 presents a magnified view of the binding site of unit 2. The binding site in the other monomer (not shown) looks very similar. The figure is aligned so as to comply as much as possible with Fig. 4 in Ref. 13. All vital interactions between both the N-terminal peptide and NPII (Ref. 12) and between OT and NPII (Ref. 13) have been conserved in our NPI/OT complex (also compare Table 2 in this work with Table 3 in Ref. 13). Moreover, the arrangements and orientations of the side chains of the amino acid residues directly contributing to the NPI/OT interface are very similar to those reported in the solid-state structures [12,13].

Figure 12 gives an idea of how well the OT tocin rings from unit 1 and unit 2 overlap each other and that in the solid-state (ss) NPII/OT structure. With the rms deviation values for the C^{α} atoms equal to 1.22, 1.51 and 1.18 Å for the unit 1/unit 2, unit 1/ss and unit 2/ss tocin ring pairs, respectively, and excellent overlap within the C1-Y2-C6 pharmacophores, it is seen that the solid-state shape of the OT part directly interacting with NPI has been perfectly reproduced in this independent modeling. On the other hand, the C-terminal ligand tail, protruding out of

TABLE 3
MATRIX OF THE RMS DEVIATIONS AMONG MODEL I, MODEL II, THE HOMODIMER AND THE 1BN2 TEMPLATE

	1BN2		Homodimer		Model II		Model I
1BN2	–		2.43		3.08		1.43
Homodimer	1.48	2.52	–		3.28		2.66
Model II	1.67	3.78	2.02	3.93	–		3.24
Model I	1.27	1.16	2.05	2.45	2.16	3.84	–

The upper triangle consists of the rms values from the overlap of all but the 1–6 NPI residues and no OT residues. The lower triangle includes double rms deviation values for each double rms cell: left values for the amino domains (residues 9–38) and right values for the carboxyl domains (residues 57–84). Since the 1BN2 file consists of only the C^{α} atom coordinates, only the C^{α} positions were subject to alignments.

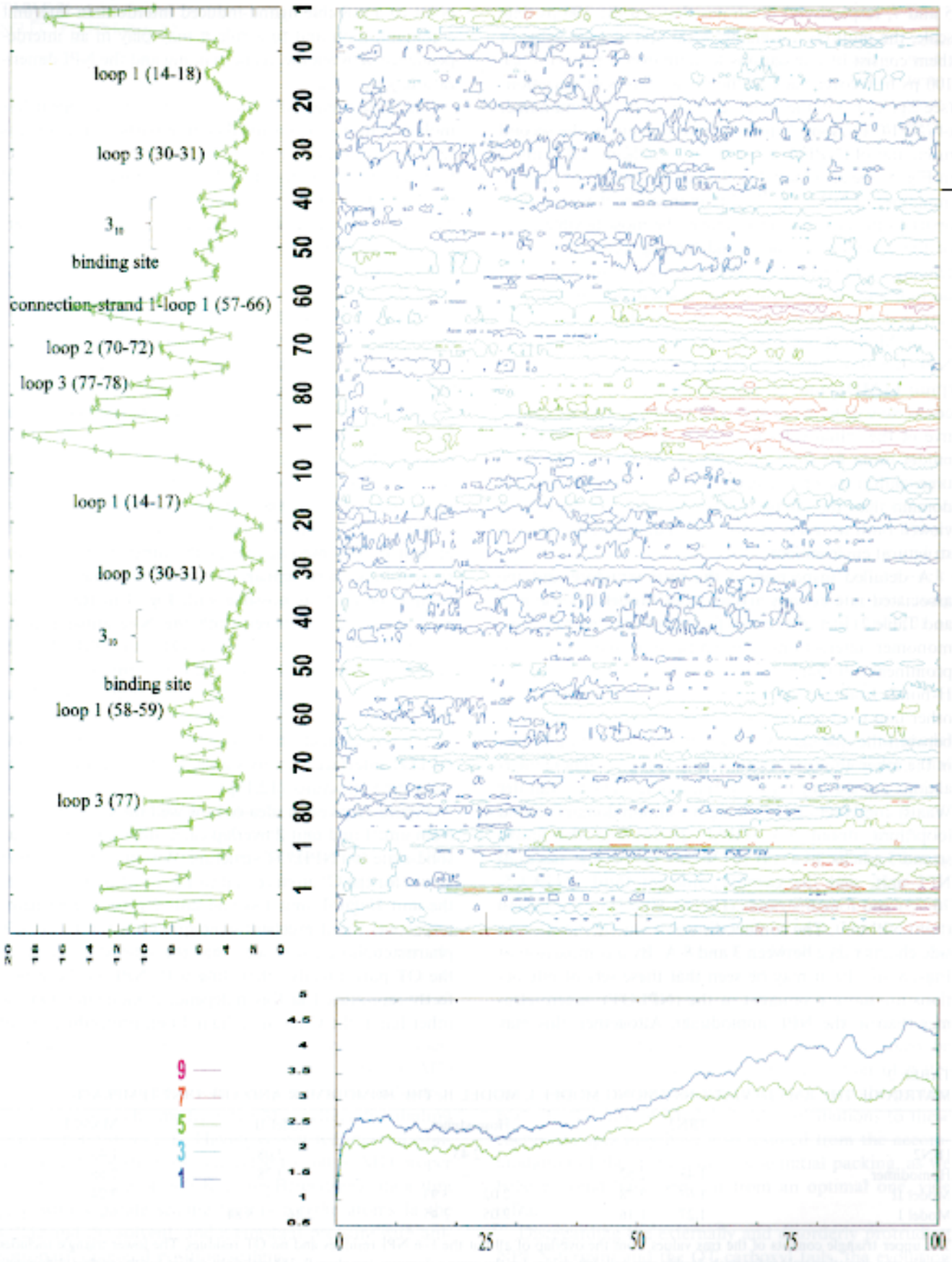

Fig. 6. The evolution of geometry in Model II over 100 ps. For details see the legend to Fig. 5.

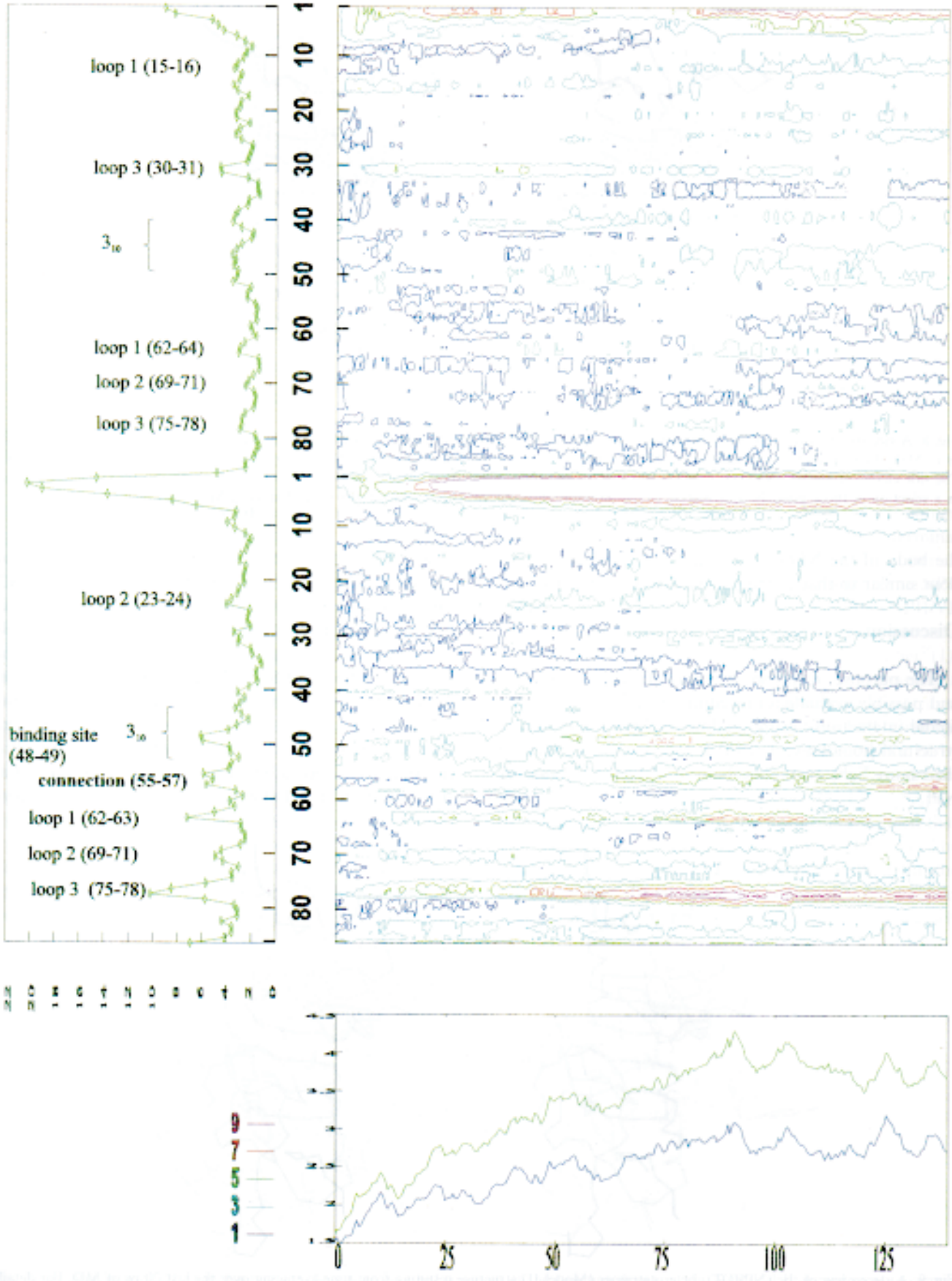

Fig. 7. The evolution of geometry in the homodimer during 136 ps. Given the absence of the OT ligand, other details are as in the legend to Fig. 5.

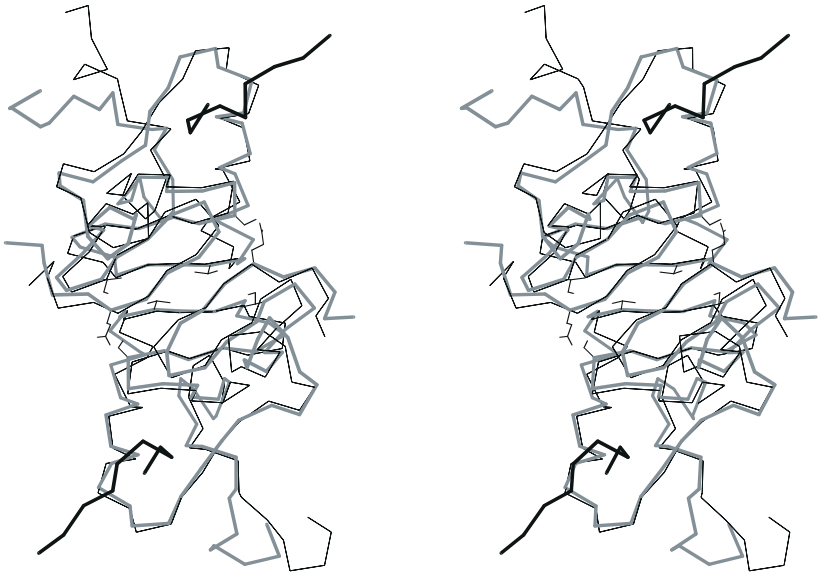

Fig. 8. A stereoview of the $(NPI/OT)_2$ heterotetramer structure obtained according to Model I and resulting from time-averaging over the last 20 ps of MD (thick gray). It is overlapping the $NPII_2$ structure taken from the Brookhaven PDB (accession code 1BN2) as a reference (thin black). The side chains of $Ser^{25}(1)$, $Val^{36}(1)$, $Asp^{81}(2)$ and $Ile^{72}(2)$, and their symmetry-related set of $Ser^{25}(2)$, $Val^{36}(2)$, $Asp^{81}(1)$ and $Ile^{72}(1)$, are indicated, as a selection of those possibly contributing to the interunit allosteric switch. The figure was generated using MolScript [22].

the body of the NPI/OT complex, has a motional freedom similar to that of the protein host's N-terminal tail.

Discussion

The purpose of this work was twofold: (i) to develop and possibly evaluate a procedure for modeling protein–ligand interactions, using the low-resolution data and/or structural homology; and (ii) if this succeeded, then to shed more light on the mechanism of ligand binding by NPI.

Regarding the first task, we suggest an optimal way for the refinement of the low-resolution data (like e.g. a C^{α} carbon atom trace) to consist of the following steps: (i) Conversion of the low-resolution data into its row all-atom representation by using, for example, SYBYL or the INSIGHT/DISCOVER [24] Biopolymer module. (ii) Careful scrutiny for the purpose of introducing obvious corrections (constraints) in the all-atom raw structure, like disulfide and/or ion bridges of known topology, Xxx-Pro *cis*-peptides if known, etc. (iii) Preparation of the initial structure prior to MD by using Model I, which automat-

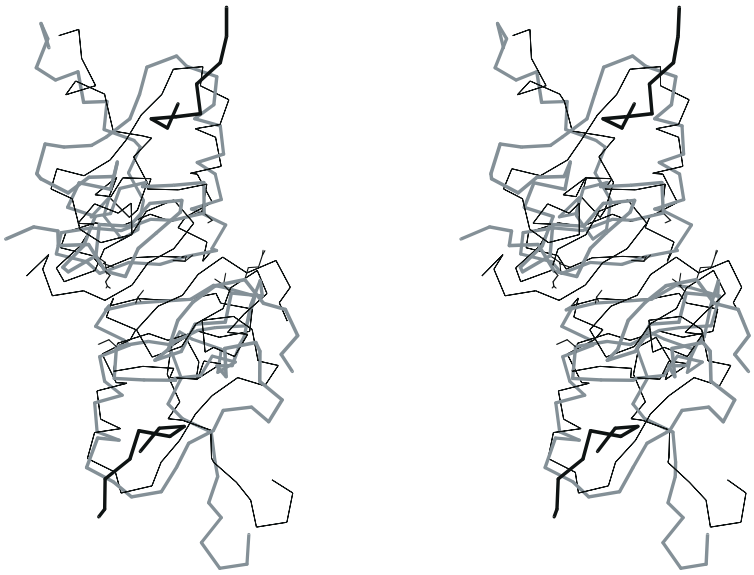

Fig. 9. A stereoview of the $(NPI/OT)_2$ heterotetramer (Model II) structure resulting from time-averaging over the last 20 ps of MD. For details see the legend to Fig. 8.

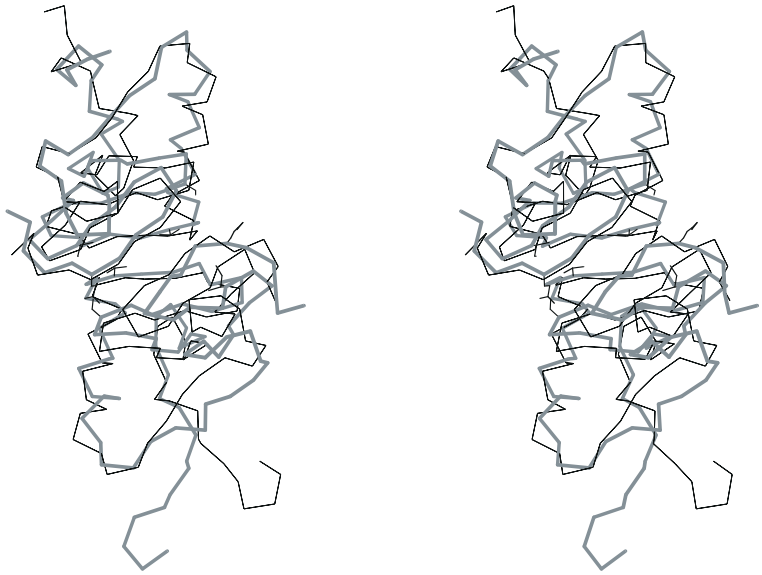

Fig. 10. A stereoview of the NPI_2 homodimer structure resulting from time-averaging over the last 20 ps of MD. For details see the legend to Fig. 8.

izes the achievement of a relaxed side-chains arrangement by an extensive use of CSA, as described in more detail in the Methods section. Steps (ii) and (iii) may need to be repeated. Procedures like Model II (see the Methods section) should be avoided as those inherent with subjectivity. (iv) Extensive MD in water. By using steps (i)–(iv), the final structures can be reproduced quite truthfully, as illustrated impressively in this work by comparisons of the OT binding sites modeled here with those recently reported in the solid-state structure.

Regarding the second task, it is clearly seen that both the $(NPI/OT)_2$ heterotetramer (Fig. 5) and the NPI_2 homodimer (Fig. 7) fluctuate quite stably over a time scale of ca. 100 ps. At the same time, an increased mobility near the ligand-binding sites in both $(NPI/OT)_2$ and NPI_2, and in the C-terminal domains of NPI_2 alone, is observed. In addition, an interesting reciprocal interaction, consisting of a strong hydrogen bond from Ser^{25} OH in the second loop of the amino domain of one monomer, to Glu^{81} COO^- in the fourth strand of the C-terminal domain of the other monomer, is observed. This interaction is present in $(NPI/OT)_2$ and half-absent in the NPI_2 dimer. This behavior was also typical of the NPII/VP complex [25]. With other interactions on the monomer–monomer interface [12–14] being unchanged, these $Ser^{25}(1)$-$Glu^{81}(2)$ and $Ser^{25}(2)$-$Glu^{81}(1)$ contacts may serve as a switching mechanism mediating the allosteric signal transfer between the ligand-binding site and the NPI dimerization. The likeliness of such a mechanism is supported by the fact that Ser^{25} immediately follows Pro^{24} in the sequence, the latter consistently believed [12,13] to be part of a tight pocket for Tyr^2 of the ligand. It is known that Tyr^2 plays a key role in ligand binding [4,12,13]. The increased mobility of the C-terminal domain may thus be correlated with the allosteric mechanism described above. Indeed, Breslow and co-workers [4,18,26] have already

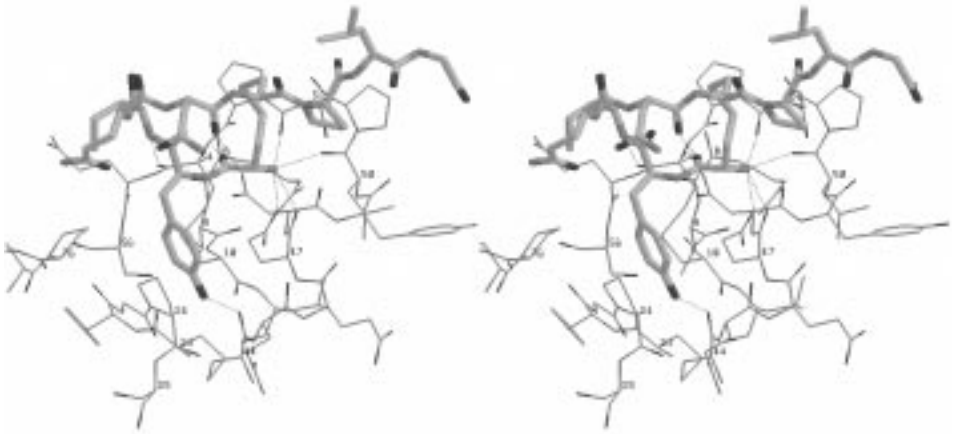

Fig. 11. A stereoview of OT in its binding site. This is an enlarged fragment of the structure drawn in Fig. 8 (Model I) aligned so as to comply as much as possible with the view in Fig. 4 of Ref. 13. The figure was generated using RasMol [23].

Fig. 12. A stereoview of three overlapping C^{α} traces of the OT structures: solid state [13] (the darkest), Model I unit 2 (medium) and Model I unit 1 (the lightest). The coordinates of the solid-state structure were obtained by scanning the stereoview (Fig. 4 in Ref. 13) and subsequent elaboration using a homemade program. The figure was generated using RasMol [23].

suggested, several times, a model in which conformational differences between unliganded monomer and dimer are important for the preferential binding of peptide to the dimer, and that the amino and carboxyl domain segments of the monomer–monomer interface, albeit homologous, are affected differently by ligand binding. Both features are reflected in our results.

Conclusions

Two methods have been described and tested for conversion of the C^{α} carbon atom trace of a protein into its all-atom structure, where CSA employing the AMBER 4.1 force field can quite reliably reproduce experimental features. This method, used to study NPI/OT interactions, was capable of pointing out specific interactions as possible candidates responsible for the allosteric communication between the ligand binding and the NPI dimerization.

Acknowledgements

This work was supported by the Polish Scientific Research Committee (KBN), grant 260/T09/96/11, by the Interdisciplinary Center for Modelling at the University of Warsaw (ICM UW), and by the Informatics Center of MAN, Gdańsk area (CI TASK).

References

1 Dreifuss, J.J., Ann. New York Acad. Sci., 248 (1975) 184.
2 Brownstein, M.J., Russell, J.T. and Ganier, H., Science, 207 (1980) 373.
3 Land, H., Schutz, G., Schmale, H. and Richter, D., Nature, 295 (1982) 299.
4 Breslow, E. and Burman, S., Adv. Enzymol., 63 (1990) 1.
5 Breslow, E. and Walter, R., Mol. Pharmacol., 8 (1972) 5.
6 Breslow, E., Annu. Rev. Biochem., 48 (1978) 251.
7 Menendez-Botet, C. and Breslow, E., Biochemistry, 14 (1975) 3825.
8 Chaiken, I.M., Randolph, R.E. and Taylor, H.C., Ann. New York Acad. Sci., 248 (1975) 442.
9 Kanmera, T. and Chaiken, I.M., J. Biol. Chem., 260 (1985) 8474.
10 Ando, S., McPhie, P. and Chaiken, I.M., J. Biol. Chem., 262 (1987) 12962.
11 Huang, H.B. and Breslow, E., J. Biol. Chem., 267 (1992) 6750.
12 Chen, L., Rose, J.P., Breslow, E., Yang, D., Chang, W.-E., Furey Jr., W.F., Sax, M. and Wang, B.-C., Proc. Natl. Acad. Sci. USA, 88 (1991) 4240.
13 Rose, J.P., Wu, Ch.-K., Hsiao, Ch.-D., Breslow, E. and Wang, B.-C., Nat. Struct. Biol., 3 (1996) 163.
14 Kaźmierkiewicz, R., Czaplewski, C., Lammek, B., Ciarkowski, J. and Lesyng, B., J. Mol. Model., 1 (1995) 135.
15 Bernstein, F.C., Koetzle, T.F., Williams, G.J., Meyer, E.E.J., Brice, M.D., Rodgers, J.R., Kennard, O., Shimanouchi, T. and Tsanumi, M., J. Mol. Biol., 112 (1977) 535.
16 SYBYL, v. 6.1, Tripos Inc., St. Louis, MO, U.S.A., 1994.
17 Lippens, G., Hallenga, K., Van Belle, S., Wodak, S.J., Nirmala, N.R., Hill, P., Russel, K.C., Smith, D.D. and Hruby, V.J., Biochemistry, 32 (1993) 9423.
18 Breslow, E., Sardana, V., Deeb, R., Barbar, E. and Peyton, D.H., Biochemistry, 34 (1995) 2137.
19 AMBER 4.1, Pearlman, D.A., Case, D.A., Caldwell, J.W., Ross, W.S., Cheatham III, T.E., Ferguson, D.M., Seibel, G.L., Singh, U.C., Weiner, P.K. and Kollman, P.A., University of California, San Francisco, CA, U.S.A., 1995.
20 Jorgensen, W.L., Chandresekhar, J., Madura, J., Impey, R. and Klein, M., J. Chem. Phys., 79 (1983) 926.
21 Berendsen, H.J.C., Postma, J.P.M., van Gunsteren, W.F., DiNola, A. and Haak, J.R., J. Chem. Phys., 81 (1984) 3684.
22 Kraulis, P., J. Appl. Crystallogr., 24 (1991) 946.
23 RasMol, v. 2.6, Molecular Visualisation Program, Sayle, R., Glaxo Wellcome Research and Development, Stevenage, Hertfordshire, U.K.
24 INSIGHT/DISCOVER, Biosym Technologies Inc., San Diego, CA, U.S.A., 1994.
25 Kaźmierkiewicz, R. et al., QSAR, (1997) in press.
26 Breslow, E., In Gross, P., Richter, G. and Robertson, G.L. (Eds.) Vasopressin, John Libbey Eurotext, Paris, France, 1993, pp. 143–155.